VIDEO OVERVIEW:
https://youtu.be/dggcGQeGbCw

IEEE ROBOTICS AND AUTOMATION LETTERS, VOL. 2, NO. 2, APRIL 2017

Serially Actuated Locomotion for Soft Robots in Tube-Like Environments

Mark D Gilbertson, Gillian McDonald, Gabriel Korinek, James D Van de Ven, and Timothy M Kowalewski

***Abstract*—Soft robots are able to complete tasks that traditional robots cannot, thus providing new opportunities for robots to navigate confined spaces. These tasks include pipe inspection and endoluminal surgical applications. The research objective of this letter is to present a design methodology for soft robots capable of traversing a cannula or pipe using only passive elements, a single pressure source, and while avoiding blockage, that is, avoiding full occlusion of the cannula to still allow fluid flow. The robot consists of three segments, each with actuators and valves, and is driven by hydraulics (water). The actuators were built using the FREE method and optimized for the specific task of traversing a cannula with a diameter of 19 mm. An experimental approach was used to create a pressure–volume relationship from the kinematic fiber-reinforced elastomer enclosure (FREE) model. The passive valves were built as flow restrictors and modeled with the nonlinear orifice equation. A simulation and grid search was performed over a range of valve coefficients. An objective function was then maximized to produce orifice coefficients that augmented extension of the robot per input pressure cycle. The physical robot was then constructed and tested in a cannula. This resulted in a robot that was serially actuated, never fully occluded the cannula, and was able to successfully locomote a cannula at a rate of 27 $\pm$ 4 mm per two-second cycle. This experimental result was close to the simulated result of 28 mm per cycle.**

***Index Terms*—Flexible robots, hydraulic/pneumatic actuators, serial actuation, soft material robotics.**

I. Introduction

SOFT robots provide opportunities to complete tasks that traditional, rigid robots cannot. By conforming manipulators to unknown, dynamic environments, soft robots are able to traverse a multitude of tight spaces within debris, construction sites, and the human body [1].

Soft robotics research was spurred in the 1950s with the invention of the McKibben actuator [2]. The McKibben actuator consists of an elastomeric tube with equal and opposite fiber wrappings allowing it to either expand or contract as an internal pressure is applied. Since that time, several kinematic and dynamic models have been created that map input pressure to an output force [3], [4]. Recent research has made substantial advances in this area by exploring the application of various wrap angles to produce novel bending, twisting, spiral, and screw motions [5]. These actuators, along with the McKibben actuators, are known as fiber-reinforced elastomer enclosures (FREEs), which map an input volume to a specified motion and address the longstanding problem of weak forces in soft robots [6]–[9].

Several studies have focused on combining multiple soft robotic actuators that are individually controlled via a fluid drive line to each actuator. One such robot consists of four fiber-reinforced actuators and four pressure inputs to navigate a cannula [10]. However, multiple drive lines make it difficult to scale the robot for intravascular or small-channel environments. Moreover, multiple drive lines require numerous pumps or controlled valves at the source, adding both bulk and cost. This underscores a need for serially-actuated soft robots, with a single control line providing an actuation medium to each actuator of the robot. In addition to the need for serial actuation, actuators must undergo reshaping, like forming spirals or extenders, that allows cannular flow to be maintained throughout locomotion.

Prior work by Ikuta *et al.* has focused on creating bandpass valves to serially actuate and control two soft bender actuators while traversing a blood vessel phantom [11], [12]. The bandpass valves were constructed via micro stereolithography and consisted of two check valves that were able to open or close to the actuator based on the input pressure from the control line [13]. A second bandpass valve by Napp *et al.* consisted of rubber flaps sandwiched between plastic orifice plates to create a two-way check valve [14].

The design of the actuators, along with the control of the dynamic response of each segment of the robot, plays an important role in achieving inherently safe, serially actuated locomotion throughout cannular networks. Previous work has focused on the serial control using complex valves, which can be difficult to scale and result in slower locomotion. However, in this letter we aim to close the existing gap in current soft robots by producing a serially actuated, soft robot using passive elements (valves) while simultaneously allowing flow throughout locomotion in tube-like environments.

The novel contribution of this letter is a generalizable method for designing soft robots to locomote through a specific tube geometry that simultaneously: (1) uses only passive components with no moving parts (i.e. simple orifice valves, unlike [14]), (2)

Manuscript received September 10, 2016; accepted January 6, 2017. Date of publication February 1, 2017; date of current version March 1, 2017. This letter was recommended for publication by Associate Editor L. Bascetta and Editor P. Rocco upon evaluation of the reviewers' comments. This work was supported by the MnDRIVE Robotics, Sensors, and Advanced Manufacturing initiative for financial support. Additionally, this material is based upon work supported by the National Science Foundation Graduate Research Fellowship Program under Grant 00039202.

The authors are with the Department of Mechanical Engineering, University of Minnesota, Minneapolis, MN 55455 USA (e-mail: gilbe767@umn.edu; mcdo0658@umn.edu; kori0019@umn.edu; vandeven@umn.edu; timk@umn.edu).

Color versions of one or more of the figures in this letter are available online at http://ieeexplore.ieee.org.

Digital Object Identifier 10.1109/LRA.2017.2662060

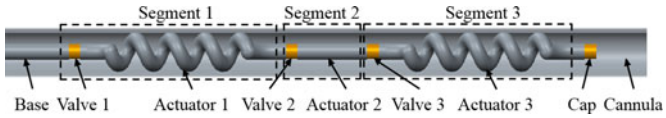

Fig. 1. Soft robot locomoting through a cannula. The robot consists of a tethered base and three segments, each containing a valve and an actuator. The spiral shapes prevent blockage of fluid flow. The cap represents the end effector.

is serially actuated (i.e. requires only one power source, unlike [10]), and (3) utilizes a geometry that avoids blocking flow while maintaining high contact area for anchoring force (i.e. a spiral actuator unlike a balloon [10] or bending actuator [13]). This includes experimental validation.

The layout of this work is as follows. First, in Section II-A of the Methods, we discuss the design of the robot based on ideal and theoretical models. In Section II-B, we discuss the modeling the actuators and valves which make up the robotic segments. Objectives will be set for the actuators and valves such that optimal robot locomotion is achieved. In Section II-C, we specify the task of the robot including the desired geometry, pressures, and dynamic response. In Sections II-D and II-E, we present the necessary actuator and valve designs needed to achieve the task, respectively. We conclude the letter with a discussion of the experimental results and future work.

II. Methods

A. Overall Design

1) Ideal Robot Design: The goal of this letter was to produce a design method for a soft robot capable of traversing a cannula through serial actuation as shown in Fig. 1. The proposed robot consisted of three segments, each including an actuator and a valve. The first and third segments contained spiral actuators to anchor into the cannular wall, while the second segment utilized an extending actuator to produce locomotion. A spiral geometry was chosen to allow locomotion to occur while also making the robot adaptable to environments where flow through the cannula must be maintained (e.g. vasculature procedures, pipe inspection).

The serial combination of the multiple segments and the control of the flow into each actuator with the valves provided the rationale for the ideal locomotion sequence represented by the events labeled in Fig. 2. Within the ideal sequence, the robot starts in its nominal unactuated state (Fig. 2 event A), then the first segment actuates, forming a spiral and anchoring into the wall of the cannula (Fig. 2 event B). While the first actuator remains anchored, the second segment actuates, causing extension along the cannula (Fig. 2 event C). This is followed by the actuation of the third segment (Fig. 2 event D). To move the robot along the cannula, the actuators are deflated in the same order of actuation (Fig. 2 events E-G). This sequence is repeated until the robot reaches its destination.

Fig. 2(b) shows the ideal timing of each actuator which corresponds to the states in Fig. 2(a). The volume-time relationship is crucial because the volume of liquid within each actuator directly translates to the pose of that actuator. There are two important volumes for the actuators. The first is the contact volume,

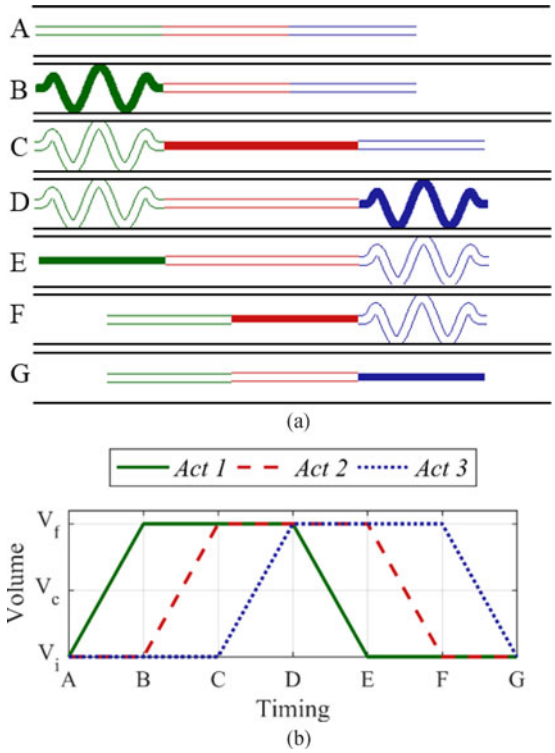

Fig. 2. (a) Ideal actuation and timing events of the soft robot actuators. (b) Volume response of each actuator corresponding to the ideal actuation events (Events labeled A-G).

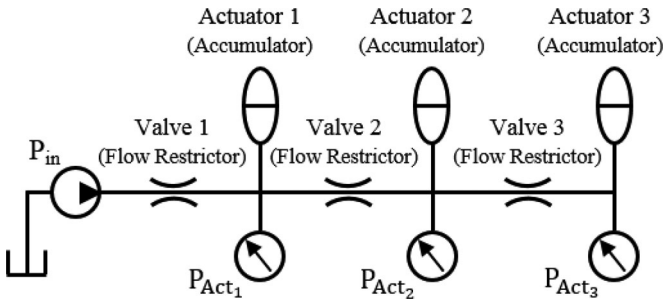

Fig. 3. Theoretical model showing each segment modeled as a flow restrictor and an accumulator.

V_c, which is the volume at which the spiral actuators (*Act 1*, *Act 3*) make contact with the cannula wall. The second important volume is the final volume, V_f, which represents fully anchored spirals for *Act 1* and *Act 3*, and a fully extended actuator for *Act 2*.

2) Theoretical System Model: For the purpose of modeling the pressures and volumes within the system, the valves were modeled as flow restricting orifices, and the actuators were modeled as nonlinear-spring-loaded hydraulic accumulators (Fig. 3).

The robot was driven by a pressure source. The resulting volume change for each segment was described by the following system of differential equations for the flow rates:

$$\begin{aligned}
\dot{V}_1 &= f_{\text{valve}_1}(u, P_{\text{Act}_1}) - f_{\text{valve}_2}(P_{\text{Act}_1}, P_{\text{Act}_2}) \\
\dot{V}_2 &= f_{\text{valve}_2}(P_{\text{Act}_1}, P_{\text{Act}_2}) - f_{\text{valve}_3}(P_{\text{Act}_2}, P_{\text{Act}_3}) \\
\dot{V}_3 &= f_{\text{valve}_3}(P_{\text{Act}_2}, P_{\text{Act}_3})
\end{aligned} \tag{1}$$

where u is the pressure input, f_{valve_i} describes the flow through a restricted orifice, and P_{Act_i} is an equation to describe the behavior of the pressure in the ith accumulator based on its material properties.

B. Model Components

1) Actuator (Accumulator) Model: The actuator was modeled as a nonlinear-spring-loaded accumulator. The volume coefficient, V, was the independent variable defined as the ratio of final actuator volume to initial actuator volume (2) and the internal pressure, P, was the dependent variable.

$$V = \frac{V_f}{V_i} \tag{2}$$

A polynomial function (3) modeled the nonlinear-spring-loaded accumulator where the coefficients, c_n, could be estimated using least squares from pressure-volume data for each actuator. The polynomial order, n_f, was increased until a residual, res (6), less than 2.5% was reached.

$$P_{\text{Act}_i} = \sum_{n=1}^{n_f} c_n (\hat{V})^n \tag{3}$$

for n_f such that $e < 2.5\%$ where

$$(\hat{V}) = V - 1 \tag{4}$$

$$e = |\text{res}(n) - \text{res}(n-1)|/\text{res}(n-1) \tag{5}$$

$$\text{res} = \left[\sum_{t=0}^{t_f} (P - [\hat{V} \ \ldots \ \hat{V}^n][c_1 \ \ldots \ c_n]^T)^2 \right]^{1/2} \tag{6}$$

The following assumptions were made: the loading on the rubber in the nonlinear-spring-loaded accumulator was time invariant, exhibited no creep, hysteresis effects were negated [15], and that derivations from such assumptions resulted in negligible error.

2) Valve (Flow Restrictor) Model: The flow restrictors were modeled using the orifice equation (7), which described fluid flow through a restricted orifice and was governed by the valve coefficient, K_i (8), and pressure drop, ΔP [16].

$$f_{\text{valve}} = K_i \sqrt[*]{|\Delta P|} \tag{7}$$

where $\sqrt[*]{x} = \text{sgn}(x)\sqrt{|x|}$.

The valve coefficient, as determined by the orifice equation, was defined as:

$$K_i = C_d A_{\text{orf}_i} \sqrt{\frac{2}{\rho_f}} \tag{8}$$

where C_d is the discharge coefficient equal to 0.62, A_{orf_i} is the cross-sectional orifice area, ρ_f is the density of the fluid equal to 997.45 [kg m^{-3}] (at 23 °C), and i indicates the valve index. Although the orifice equation is a steady state model, we assumed this model holds true throughout actuation of the robot.

C. Physical Realization and Targeted Task

1) Task: To illustrate our general methodology, the specified task for the robot design was to locomote through a cannula ($D = 19$ mm) using a combination of segments that occluded the cannula by less than 50% and experienced pressures under 200 kPa. The timing of the actuation needed to follow Fig. 2. This meant that *Act 1* must anchor before extension of *Act 2* contributed to locomotion. Additionally, *Act 2* must be near its final volume before *Act 3* anchored. This prevents *Act 2* from buckling or wasting motion.

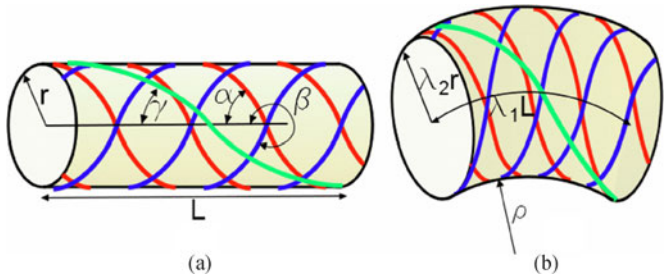

Fig. 4. FREE wrap angles and stretch parameters from Bishop-Moser *et al.* [7].

D. Actuator Design and Construction

1) Actuator Design: To achieve the desired area occlusion ratio, the actuators inner radius was chosen as $r = 5$ mm with 0.8 mm thickness, resulting in an area occlusion ratio of 37%.

To achieve the actuator shapes shown in Figs. 1 and 2, FREE actuators were used. FREE actuators utilize two or three varying wrap angles α, β, γ, as shown in Fig. 4, to create spiral or extending actuators [5], [7]. The derivation of the FREE model relied on fiber inextensibility resulting in the geometric relations in 9–11. The following derivation of (9)–(16) are attributed to and detailed in [5]–[9].

$$\lambda_1^2 c_\alpha^2 + \lambda_2^2 s_\alpha^2 \left(\frac{\theta + \delta}{\theta} \right) = 1 \tag{9}$$

$$\lambda_1^2 c_\beta^2 + \lambda_2^2 s_\beta^2 \left(\frac{\zeta + \delta}{\zeta} \right) = 1 \tag{10}$$

$$\lambda_1^2 c_\gamma^2 + \lambda_2^2 s_\gamma^2 \left(\frac{\psi + \delta}{\psi} \right) = 1 \tag{11}$$

$$\theta = \frac{L \tan(\alpha)}{r}, \zeta = \frac{L \tan(\beta)}{r}, \psi = \frac{L \tan(\gamma)}{r}$$

where $c_\alpha = \cos(\alpha)$, $s_\alpha = \sin(\alpha)$, and L represents the overall length of the actuator.

The radial stretch parameter, λ_2, and axial twist, δ, were solved as functions of the axial stretch parameter, λ_1. This was done by substituting (9) into (10), resulting in (12) and (13), respectively.

$$\lambda_2 = \frac{\frac{\alpha}{|\alpha|} c_\beta \sqrt{1 - c_\alpha^2 \lambda_1^2} - \frac{\beta}{|\beta|} c_\alpha \sqrt{1 - c_\beta^2 \lambda_1^2}}{s_{\alpha - \beta}} \tag{12}$$

$$\delta = \frac{L}{r} \frac{\frac{\beta}{|\beta|} s_\alpha \sqrt{1 - \lambda_1^2 c_\beta^2} - \frac{\alpha}{|\alpha|} s_\beta \sqrt{1 - \lambda_1^2 c_\alpha^2}}{\frac{\alpha}{|\alpha|} c_\beta \sqrt{1 - \lambda_1^2 c_\alpha^2} - \frac{\beta}{|\beta|} c_\alpha \sqrt{1 - \lambda_1^2 c_\beta^2}} \tag{13}$$

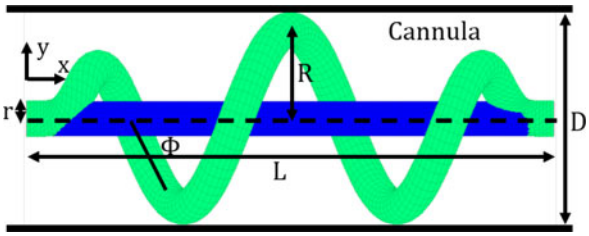

Fig. 5. Pertinent dimensions for a FREE spiral within a tube.

The volume coefficient, V, was used to obtain a solution for λ_1 and was also an input to the system. V can be expressed in terms of stretch parameters:

$$V = \lambda_1 \lambda_2^2 \tag{14}$$

To solve for λ_1, the Newton Raphson method was applied to (12) and (14) with an initial condition of $\lambda_1 = 1$ [8]. For spiral actuators consisting of three separate fiber angles, the helix radius, R (15), was defined as the radius of the spirals. The helix radius as well as the helix angle, ϕ (16), are depicted in Fig. 5 and their derivation can be found in [7].

$$R = \frac{\rho}{1 + \left(\frac{(\delta+\psi)\rho}{L}\right)^2} \tag{15}$$

$$\phi = \arctan\left(\frac{(\delta+\psi)\rho}{L}\right) \tag{16}$$

where ρ is provided in [7].

To demonstrate our generalizable method, we target actuators capable of forming the desired spiral in Fig. 1 as dictated by a specific task (i.e. traversing a $D = 19$ mm diameter tube). This informed the specific design criteria, which were fed into a cost function. The first constraint was to set the volume coefficient to $V = 1.30$ which was used for both spirals and the extending actuator. A $V = 1.30$ was chosen because it is large enough to produce the desired R and stable enough to obtain solutions before geometric lock (e.g. see [5]). For the actuator to successfully traverse a tube, R must be greater than or equal to $D/2$ (Fig. 5). The selection for this desired helix radius, $\hat{R}$, was $D/2$. This assumed traction forces large enough to anchor the actuator in the cannula since the spiral was able to compress twice the radius of the actuator on the cannular wall. Next, we aimed to maintain constant overall axial length of the spiral actuator in the x-direction, λ_x, as shown by (17). A constant value was chosen as it reduces slip between the cannula and actuator between contacting and anchoring.

$$\lambda_x = \lambda_1 L \cos(\phi)\sqrt{\cos^{-2}(\phi) - 1} \tag{17}$$

The final objective of the cost function was to minimize the axial twist, δ, of the actuator (i.e. $\hat{\delta} = 0$) to minimize shear on the tube wall and maximize the efficiency of the robot. A simple grid search with a constant step size of 1.0° was performed over all α, β, γ permutations and the linear quadratic cost function (18) was evaluated with the design parameters in Table I. The α, β, γ values that minimized cost were taken to be the optimal fiber wrap angles. The value for r was chosen based on the off-the-shelf latex tubing used to manufacture the actuators.

TABLE I
TASK-SPECIFIC DESIGN PARAMETERS FOR $D = 19$ MM

r	L	$\hat{R}$	$\hat{\lambda_x}$	$\hat{\delta}$
5 mm	300 mm	$D/2$	1.0	0.0

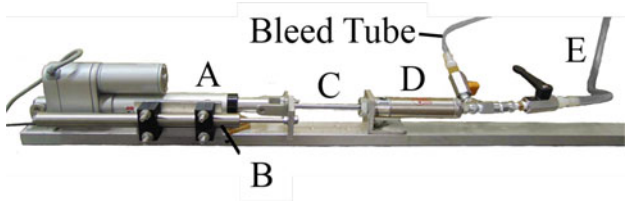

Fig. 6. Closed hydraulic circuit test bench: A) linear actuator B) LVDT C) cylinder piston rod D) stroke cylinder E) tubing leading to the FREE actuator.

$$\begin{aligned} &\underset{\Phi}{\text{minimize}} \quad \Phi^T Q \Phi \\ &\text{subject to} \quad \alpha, \beta, \gamma \in [-90, 90] \end{aligned} \tag{18}$$

where

$$\Phi = [\hat{R} - R, \hat{\lambda}_x - \lambda_x, \hat{\delta} - \delta] \tag{19}$$

$$Q = I_{3x3} \tag{20}$$

The second actuator was an extending McKibben actuator that was specified to consist of equal but opposite fiber wrappings greater than 54.7°. The goal of the second actuator was to extend without buckling. The wrap angles of the extending actuator were determined through an empirical study, which examined the relationship between wrap angle, actuator buckling, and actuator extension. The volume coefficient for this actuator was the same as the spiral design, $V = 1.30$.

To identify the parameters in (3) for the kinematic actuator model using a pressure input, an experiment was performed. The nonlinear-spring-loaded accumulator model shown in (3) was applied. Since the system was filled with water, we assumed incompressibility. The relationship between P_{Act_i} and V were found experimentally by inputting a sine wave on volume using the characterization hydraulic test bench shown in Fig. 6. The test bench recorded the volume coefficient, V, and actuator pressure, P, at 100 Hz. Eq. 3 was then applied to determine the number of coefficients and their respective values with least squares.

2) Actuator Construction: The FREE actuators were constructed by turning fibers onto a latex tube (Kent Elastomer Products, Inc.) as shown in Fig. 7. A dipping process was used to secure the wrapped fibers in place. Each wrapped actuator was dipped three times into a 50/50 distilled water-latex (TAP Plastics Premium Liquid Latex Rubber) mixture with a two hour cure time between dips.

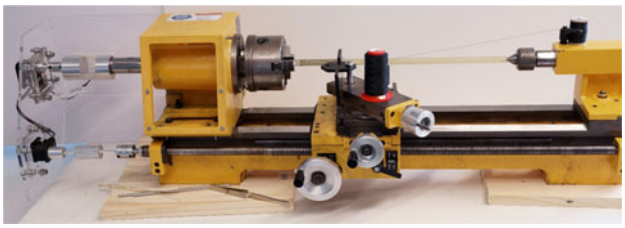

Fig. 7. Computer-controlled lathe modified to wrap fibers at desired α, β, γ wrap angles onto a latex tubing.

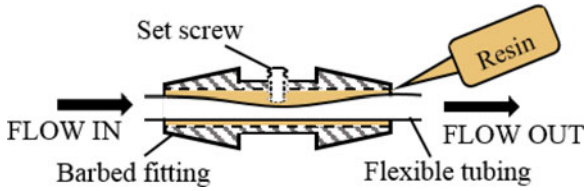

Fig. 8. A manufactured passive valve. The process used to manufacture valves is as follows: begin with a barbed fitting compatible with actuator size; insert set screw into the fitting wall; back out set screw and insert flexible tubing; fill empty space with polyurethane resin.

The stretchability of the latex tubing allowed for sufficient motion of the actuators while keeping pressures under the task specification of 200 kPa.

E. Valve Design and Construction

1) Valve Design: To create a model for the soft robot, (3) and (7) were substituted into (1) to create the dynamic equations shown in (21). The input pressure, u, was selected to be a pressure square wave between 0 and 83 kPa with a two second period.

$$\begin{aligned}\dot{V}_1 &= K_1\sqrt{u-P_1}' - K_2\sqrt{P_1-P_2}'\\ \dot{V}_2 &= K_2\sqrt{P_1-P_2}' - K_3\sqrt{P_2-P_3}'\\ \dot{V}_3 &= K_3\sqrt{P_2-P_3}'\end{aligned} \tag{21}$$

Optimization of the resulting model (21) was performed with the design parameters being the valve coefficients, K_i, of the valves. The optimization had two objectives. The first was to maximize the volume change of Act_2 while Act_1 was anchored into the cannula, t_B, and before Act_3 had contacted the cannula, t_C, during the inflation phases, V_{fwd} (22). The second goal was to maximize the volume change of Act_2 between Act_1 releasing contact from the cannula, t_E, and Act_3 unanchoring, t_F, during the deflation, V_{rev} (23). V_{fwd} and V_{rev} were then combined into a single objective function which aimed to maximize their value while keeping their volume changes the same (24). See Fig. 2 for event time labels t_B, t_C, etc.

$$V_{\text{fwd}} = V_{\text{Act}_2}(t_B) - V_{\text{Act}_2}(t_C) \tag{22}$$

$$V_{\text{rev}} = V_{\text{Act}_2}(t_E) - V_{\text{Act}_2}(t_F) \tag{23}$$

$$\begin{aligned}&\underset{K_2,K_3}{\text{maximize}} \quad J_{\text{vol}} = [V_{\text{fwd}}^2 \;\; V_{\text{rev}}^2][c_1 \;\; c_2]^T - c_3|V_{\text{fwd}} - V_{\text{rev}}|^2\\ &\text{subject to} \quad K_2, K_3 = [0, K_1]\end{aligned} \tag{24}$$

where $c_i = 1$ for $i = 1, 2, 3$.

The robot response to the chosen input was simulated using MATLAB and Simulink. The simulation utilized the nonlinear-spring-loaded accumulator model, P_{Act_i} (3), and the orifice equation, f_{valve} (7), to simulate the robot model in (1). A square wave with an amplitude of 83 kPa gauge pressure and frequency of 0.5 Hz was used as the input. The pressure was chosen based on the material characteristics of the actuator. The frequency was chosen because it was intuitive for human users and is on the order of a resting heart rate, thus avoiding subjecting anatomy to foreign frequency content. The contact and anchoring volume coefficients were defined as 1.13 and 1.30 as dictated by the actuator design.

To ensure that *Act 1* actuated as quickly as possible, the cross-sectional orifice area, A_{orf_1}, was set to its maximum value dictated by the valve geometry. This maximized the valve coefficient through valve 1. The simulation performed a grid search over K_2 and K_3 for values less than or equal to K_1 using a constant step size of 5.0×10^{-7} m^2. An optimal value for K_1 was not incorporated into the objective function because valve 1 was made to allow as much flow into *Act 1* as possible, making K_1 the largest possible value determined by the valve's cross-sectional area. Equation (24) was then evaluated and the K_2, K_3 combination which maximized J_{vol} was taken as the optimal dynamic response.

2) Valve Construction: The desired valves were constructed by placing flexible tubing within a barbed fitting, inserting a set screw into the fitting wall, then setting the tubing with cast polyurethane (TAP Plastics, One-to-One Polyurethane Casting Resin) (Fig. 8). The set screw allowed for adjustments in the flow restrictor opening, changing the effective K_i.

To match the flow restrictor with the K_i's found by the simulation, the characterization hydraulic test bench (Fig. 6) was used with the flow restrictor placed between two pressure sensors. A cascading set of steps on voltage were inputted to the linear actuator, while the pressure drop, ΔP, and piston position were recorded. The data was then filtered with a 4th order Butterworth filter with a cutoff frequency of 10 Hz. Next, the data was segmented for each voltage and transients were removed by attributing the data collected during the first third of the stroke length to acceleration and evaluating the remaining data from the last two thirds of the stroke length. The flow rate was then calculated using a noise robust differentiation [17] based on the segmented piston position. Least squares was then applied to determine the K_i term of the flow restrictor. If the K_i found using the test bench was above (or below) the desired K_i, the set screw on the flow restrictor was tightened (or loosened). This process was repeated until the target K_i from the simulation was achieved within 2%.

3) Robot Locomoting Through a Tube: Once all the valves were tuned and the actuators were built, each segment was assembled and combined to form the robot. The locomotion hydraulic test bench was connected to the robot and used as a pressure source. A 0.5 Hz square wave input with an amplitude of 83 kPa was implemented with the locomotion hydraulic test bench. The robot was then placed in a cannula of diameter

TABLE II
ACTUATOR WRAP ANGLES

	α	β	γ
Spiral	72°	-72°	-14°
Extender	80°	-80°	–*

*wrap angle not used.

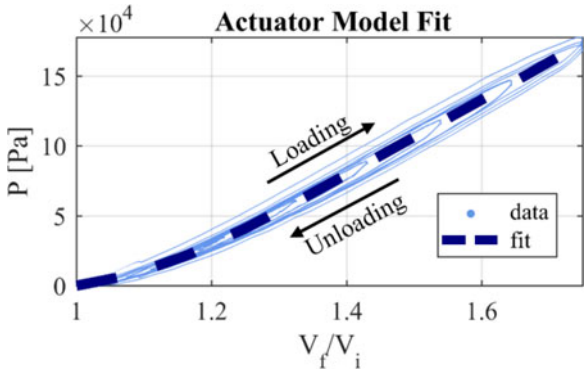

Fig. 9. Nonlinear-spring-loaded accumulator relationship shown with a hysteresis loop for actuator 1.

TABLE III
PRESSURE VOLUME RELATIONSHIP FOUND WITH (3)

	c_1	c_2	c_3	c_4
P_{Act_1}	1.60	5.92	−11.14	7.18
P_{Act_2}	0.44	6.64	−8.79	4.28
P_{Act_3}	−0.28	10.61	−12.39	5.06

$D = 19$ mm and the segments were inflated and deflated to produce locomotion. A panel of reviewers ($N = 6$) identified key timing events over 5.5 cycles of locomotion recorded at 24 fps 1080P (Cannon EOS Rebel T6).

III. RESULTS

A. Actuator (Accumulator) Models and Design Outputs

The α, β, γ wrap angles which optimized cost objectives specified by the design tasks and extender empirical study are shown in Table II.

Fig. 9 shows the experimental results from the nonlinear-spring-loaded accumulator experiment for a single spiral actuator. The same protocol was repeated for the other two actuators and the resulting coefficients are listed in Table III. However, the pressure volume relationship for each actuator followed similar curves and values.

B. Valve Results

The simulation produced an objective function showing the values of J_{vol} (24) for each combination of K_i's in the grid search (Fig. 10).

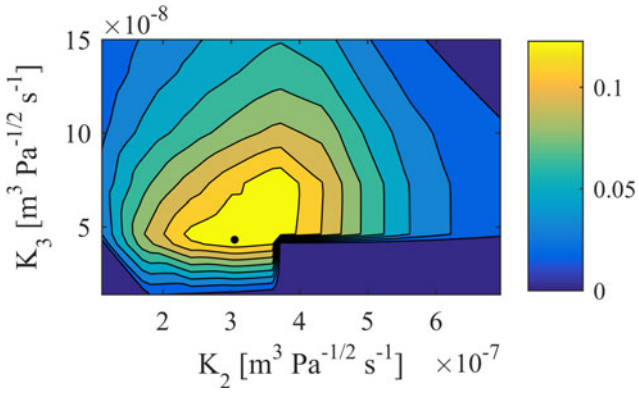

Fig. 10. Objective function of grid search performed over K_i values, where the black dot represents the maximum of (24).

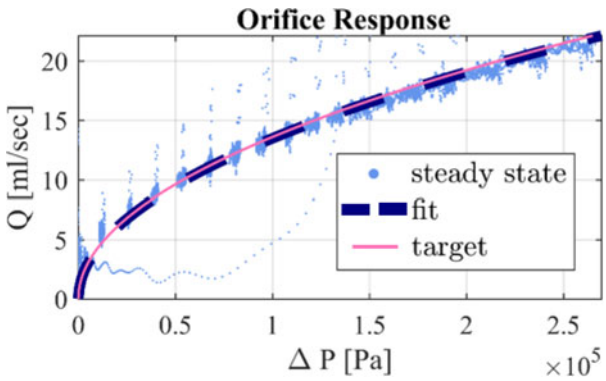

Fig. 11. Flow restrictor testing and models shown for valve 3 (transparency for steady state data set to 15%; transient data excluded).

TABLE IV
VALVE RESISTANCE

K_i [m^3 Pa$^{-1/2}$ s^{-1}]	Valve 1	Valve 2	Valve 3
Optimal	1.64×10^{-6}	3.05×10^{-7}	4.30×10^{-8}
Fit	–*	3.02×10^{-7}	4.26×10^{-8}
Error	–*	−1.04%	−0.84%

*determined by max cross section.

The values of K_i correlating to the maximum of the objective function were matched experimentally. The experimental change in pressure versus flow data for each flow restrictor was compared to the optimal pressure versus flow data. An example of the experimental response versus optimal response can be seen in Fig. 11. The final values for both the optimal and experimental K_i values are shown in Table IV.

After finding the optimal K_i values using the objective function shown in Fig. 10, the values were entered into the simulation to produce the optimized volumetric response (Fig. 12) where V_{fwd} and V_{rev} both took 140 ms. Due to the different polynomial constants describing each accumulator, the final volume coefficients vary.

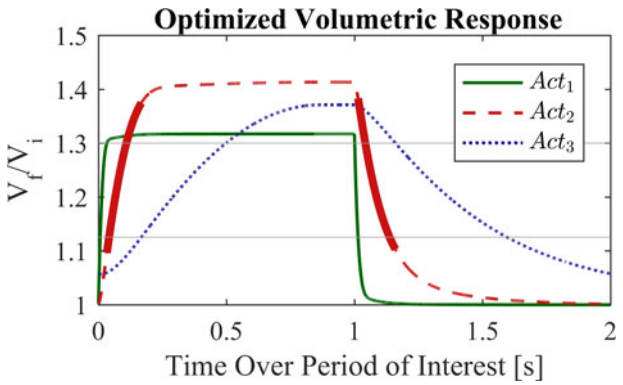

Fig. 12. Optimized volumetric response for half an actuation period. States corresponding to Fig. 2 (a, b) are shown, with the extender volume objective (24) highlighted in bold for *Act 2*. ($V_i = 1.00$, $V_c = 1.12$, $V_a = 1.30$); (Event timings: $t_A = 0.00$ s, $t_B = 0.03$ s, $t_C = 0.17$ s, $t_D = 1.00$ s, $t_E = 1.02$ s, $t_F = 1.16$ s, $t_G = 2.00$ s).

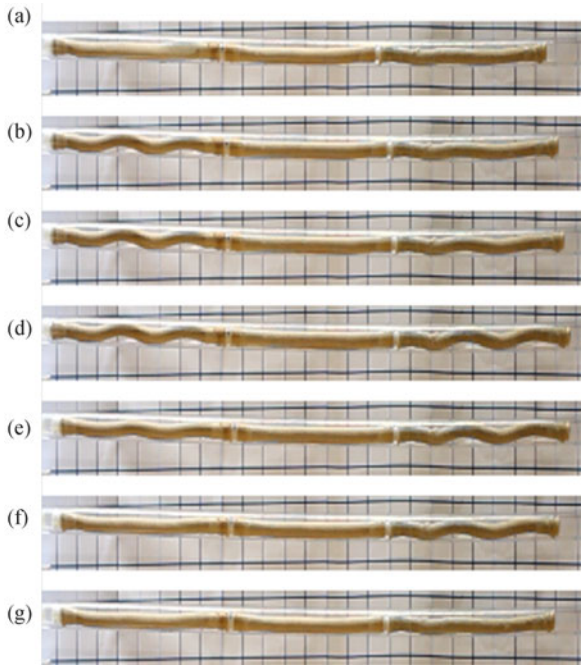

Fig. 13. Soft robot at each event (Labeled A-G) in a cannula for a full cycle of 2 seconds. (Compare with Fig. 2) The grid markings in this figure and Fig. 14 are 5 mm by 5 mm, the image was cropped and the horizontally shrunk by 35%.

C. Soft Robot Modeling

The soft robot successfully traversed the cannula as shown in Fig. 13. The robot locomoted 27 $\pm$ 4 mm for each actuation cycle, which is within the deviation of the predicted locomotion of 28 mm. Fig. 14 shows the robot locomoting through the cannula at different time steps, allowing one to view the traversal. For both Figs. 13 and 14, a 5 mm by 5 mm grid can be seen in the background. The images were cropped and the image was shrunk to 35% of its original size in the horizontal direction. Additionally, the median timing of actuation was within the measurement resolution of the prescribed timing as shown in Fig. 15.

Fig. 14. Soft robot locomotion through a cannula at different time steps. The images were captured at full anchoring, Event D (See Figs. 2(a) and 13).

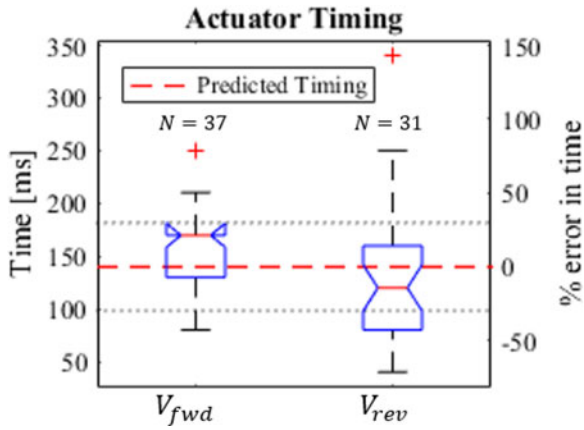

Fig. 15. Experimental actuator timing for the forward, ($t_C - t_B$), and reverse, ($t_F - t_E$), direction. Results found with ($N = 6$) independent reviewers timing all events for ($N = 37$) and ($N = 31$). The dotted black measurement lines represent the discrete measurement resolution with a video being recorded at 24 frames per second. Notches represent range in significant difference in median at $p = 0.05$.

IV. Discussion

We successfully used methodology proposed in [7] to provide ideal wrap angles for each actuator in our robot (Table II). The spiral actuator closely met the objectives described in Table I. The actuator pressure-volume relationship (Fig. 9) was nonlinear and exhibited some rate-independent hysteresis. This deviated from our assumptions, but not substantially relative to the full pressure-volume range.

The optimization of the extension volume implies useful forward traversal locomotion. In general, the last orifice (K_3) has greater impedance than (K_2) meaning that optimal tuning is more sensitive to changes in (K_3) than (K_2).

The resulting optimization (Fig. 12) shows that well over 50% of the extension volume change results in extension as well as roughly equal and useful expansion and retraction stages. One thing to note is that *Act 3* always has a volume coefficient greater than one. This is due to the system reaching a cyclic steady state response and *Act 3* not being able to fully deflate. It is worth noting that all three actuators have different coefficients (see Table III) and different final volumes ($V_f/V_i > 1.3$ in Fig. 12) because the dipping processes was not fully repeatable resulting in slightly different wall thicknesses.

The use of the orifice equation (7) to model the valves was mostly justified as seen in Fig. 11 with the exclusion of most transient data.

The experiment showed that the proposed design methodology succeeded at a) creating shapes and sequences proposed in Figs. 1 and 2, b) achieved the timing suggested in Fig. 2(b) and c) resulted in overall locomotion that was serially actuated and, by design, avoided full occlusion of the cannula cross section thus allowing fluid flow. The actuator timing, when accounting for measurement resolution, proved quite accurate since the mean timing for the forward and reverse direction fell within one frame of the specified timing. Errors in the timing could be attributed to the effect of external loading due to the contact and anchoring in the cannula. The effect on the system's dynamics can be seen in Fig. 15. During inflation, the actuator is fighting the reaction force generated due to contacting the cannula, thus extending the time period of V_{fwd}. Conversely, the time period of V_{rev} is shorter due to the reaction force assist the deflation gets from contact with the cannula. Our model neglected this contact interaction, however, the resulting deviation was minimal (i.e. did not prevent locomotion).

V. Conclusion

We presented and experimentally verified a design methodology to realize task-specific, serially actuated soft robots to traverse tube-like environments without causing full occlusion of the tubular cross section. While we demonstrated this work for a specific case, it is generalizable to other applications and environments. Such methodology can benefit multiple applications including pipe inspection and medical catheter robots.

Currently, the methodology does not include sensing and navigation control, but instead focuses on locomotion only. Consequently, the soft robot could locomote through bends, but would need an additional degree of freedom to choose a particular path upon coming to a junction.

The work presented has room for advancement. A study of occlusion ratio and pressure drop in pipe flow will need to be evaluated. A traction model predicting the slip between the spiral and cannula wall and effects on inflation as well as buckling or out plane motion of the extender could be developed to greatly improve the accuracy of the predicated locomotion. Additionally, the optimization can expand to include actuation frequency and actuator stiffness to tune robot designs for different environments and actuator timing.

References

[1] D. Rus and M. T. Tolley, "Design, fabrication and control of soft robots," *Nature*, vol. 521, no. 7553, pp. 467–475, May 2015.

[2] G. Andrikopoulos, G. Nikolakopoulos, and S. Manesis, "A survey on applications of pneumatic artificial muscles," in *Proc. Mediterranean Conf. Control Autom.*, Jun. 2011, pp. 1439–1446.

[3] C.-P. Chou and B. Hannaford, "Measurement and modeling of Mckibben pneumatic artificial muscles," *IEEE Trans. Robot. Autom.*, vol. 12, no. 1, pp. 90–102, Feb. 1996.

[4] B. Tondu, "Modelling of the Mckibben artificial muscle: A review," *J. Intell. Mater. Syst. Struct.*, vol. 23, no. 3, pp. 225–253, Mar. 2012.

[5] J. Bishop-Moser and S. Kota, "Design and modeling of generalized fiber-reinforced pneumatic soft actuators," *IEEE Trans. Robot.*, vol. 31, no. 3, pp. 536–545, Jun. 2015.

[6] J. L. Bishop-Moser, "Design of generalized fiber-reinforced elasto-fluidic systems," Ph.D. dissertation, Dept. Mech. Eng., Univ. Michigan, Ann Arbor, MI, USA, 2014.

[7] J. Bishop-Moser and S. Kota, "Towards snake-like soft robots: Design of fluidic fiber-reinforced elastomeric helical manipulators," in *Proc. IEEE/RSJ Int. Conf. Intell. Robots Syst.*, Nov. 2013, pp. 5021–5026.

[8] G. Krishnan, "Kinematics of a new class of smart actuators for soft robots based on generalized pneumatic artificial muscles," in *Proc. IEEE/RSJ Int. Conf. Intell. Robots Syst.*, Sep. 2014, pp. 587–592.

[9] G. Krishnan, J. Bishop-Moser, C. Kim, and S. Kota, "Evaluating mobility behavior of fluid filled fiber-reinforced elastomeric enclosures," in *Proc. ASME Int. Des. Eng. Tech. Conf.*, Aug. 2012, pp. 1089–1099.

[10] F. Connolly, P. Polygerinos, C. J. Walsh, and K. Bertoldi, "Mechanical programming of soft actuators by varying fiber angle," *Soft Robot.*, vol. 2, no. 1, pp. 26–32, Mar. 2015.

[11] K. Ikuta, M. Matsuda, D. Yajima, and Y. Ota, "Precise bending angle control of hydraulic active catheter by pressure pulse drive," in *Proc. IEEE Int. Conf. Robot. Autom.*, May 2010, pp. 5588–5593.

[12] K. Ikuta, Y. Matsuda, D. Yajima, and Y. Ota, "Pressure pulse drive: A control method for the precise bending of hydraulic active catheters," *IEEE/ASME Trans. Mechatron.*, vol. 17, no. 5, pp. 876–883, Oct. 2012.

[13] K. Ikuta, H. Ichikawa, K. Suzuki, and D. Yajima, "Multi-degree of freedom hydraulic pressure driven safety active catheter," in *Proc. IEEE Int. Conf. Robot. Autom.*, May 2006, pp. 4161–4166.

[14] N. Napp, B. Araki, M. T. Tolley, R. Nagpal, and R. J. Wood, "Simple passive valves for addressable pneumatic actuation," in *Proc. IEEE Int. Conf. Robot. Autom.*, May 2014, pp. 1440–1445.

[15] E. B. Tadmor, R. E. Miller, and R. S. Elliott, *Continuum Mechanics and Thermodynamics: From Fundamental Concepts to Governing Equations*. Cambridge, U.K.: Cambridge Univ. Press, 2012.

[16] J. S. Cundiff, *Fluid Power Circuits and Controls: Fundamentals and Applications*. Boca Raton, FL, USA: CRC Press, 2001.

[17] P. Holoborodko, "Smooth noise robust differentiators," 2008. [Online]. Available: http://www.holoborodko.com/pavel/numerical-methods/numerical-derivative/smoo th-low-noise-differentiators/